JOURNAL OF AIRCRAFT
Vol. 42, No. 3, May–June 2005

F/A-18C to E Wing Morphing Study for the Abrupt-Wing-Stall Program

Bradford E. Green*
U.S. Naval Air Systems Command, Patuxent River, Maryland 20670
and
James D. Ott†
Combustion Research and Flow Technology, Inc., Pipersville, Pennsylvania 18947

In an effort to determine the impact of various wing parameters on the abrupt-wing-stall phenomenon encountered by the preproduction F/A-18E, various characteristics of the F/A-18C wing were modified to reflect the design changes incorporated into the F/A-18E wing. The parameters evaluated during this computational study included thickness, camber, twist, leading-edge radius, leading-edge flap-chord ratio, and the addition of a leading-edge snag. After modifying the wing parameters independently and then in combination, a computational-fluid-dynamics flow solver was used to evaluate the computational grids. A figure of merit was then used to determine the impact of the various wing parameters on the abrupt stall. Several potential computational figures of merit were evaluated to determine their utility for the prediction of an abrupt wing stall. One of the most promising figures of merit for indicating the onset of an abrupt stall was found to be the wing-root bending-moment coefficient. Using this figure of merit, it was determined that the incorporation of a leading-edge snag, the reduction of leading-edge flap-chord ratio and the elimination of camber are the likely contributors to the abrupt-stall phenomenon encountered by the aircraft.

Nomenclature

b	=	wing span, ft
C_D	=	aircraft drag coefficient, $D/(q_\infty S)$
C_L	=	aircraft lift coefficient, $L/(q_\infty S)$
C_p	=	static pressure coefficient, $(P - P_\infty)/(q_\infty)$
C_{WB}	=	wing-root bending-moment coefficient
c	=	chord of wing airfoil section, ft
c_l	=	sectional lift coefficient, $l/(q_\infty c)$
D	=	drag on aircraft, lb
L	=	lift on aircraft, lb
l	=	wing sectional lift, lb/ft
P	=	static pressure, lb/ft^2
q_∞	=	dynamic pressure, $(0.5\rho_\infty U_\infty^2)$, lb/ft^2
Re	=	Reynolds number, $(\rho_\infty U_\infty c_{\mathrm{mac}})/\mu_\infty$
S	=	wing reference area, ft^2
U_∞	=	freestream velocity, ft/s
x	=	chordwise distance along wing, ft
y	=	spanwise distance along wing, ft
α	=	angle of attack, deg
μ_∞	=	freestream dynamic viscosity, slugs/ft-s
ρ_∞	=	freestream density, slugs/ft^3

Subscripts

mac	=	mean aerodynamic chord
ref	=	reference
root	=	wing root
tip	=	wing tip
∞	=	freestream

Presented as Paper 2003-0925 at the AIAA 41st Aerospace Sciences, Reno, NV, 6–9 January 2003; received 5 June 2003; revision received 14 August 2003; accepted for publication 9 September 2003.

*Aerospace Engineer, Air Vehicle Engineering Department, Aeromechanics Division, Building 2187, Unit 5, Suite 1320-B, 48110 Shaw Road; bradford.green@navy.mil. Member AIAA.

†Research Scientist, 6210 Keller's Church Road, Pipersville, Pennsylvania 18947; ottjd@craft-tech.com. Member AIAA.

Introduction

DURING the engineering and manufacturing development phase of the F/A-18E/F program, preproduction aircraft encountered an uncommanded, abrupt rolling motion during transonic maneuvering conditions.[1] Commonly referred to as abrupt wing stall (AWS), this phenomenon occurs when there is a loss in roll damping or when the amount of flow separation on the upper surface of the wings increases rapidly and asymmetrically. A rolling moment results from the difference in lift that is generated between the two wings. Abrupt stall degrades the tracking capability of the aircraft and causes safety concerns if it occurs at low altitudes.[2]

Modifications of the automatic leading-edge flap schedule and the addition of a porous surface at the wing fold solved the abrupt stall problem on the F/A-18E/F and were incorporated into the production versions of the aircraft. As a result of the modifications, the F/A-18E/F's being delivered to the fleet are no longer susceptible to AWS. On the recommendation of a high level panel that overviewed the technical problems encountered in the early development program, the AWS program was formed to obtain a better understanding of the causes of abrupt stall.[1] The AWS program is a national team composed of the U.S. Navy, NASA, U.S. Air Force, and several universities. The research presented in this paper was funded through the AWS program.

The reader is cautioned that references to the F/A-18E configuration herein are to the preproduction configuration without the wing modifications. In particular, the current study was for an aircraft without porosity.

There are significant differences in the wing characteristics between the F/A-18C and the F/A-18E. During the development of the F/A-18E, changes were made to the wing by modifying the thickness, camber, twist, leading-edge radius, leading-edge flap-chord ratio, and adding a leading-edge snag. The differences in these wing parameters between the F/A-18C and the F/A-18E are shown in Table 1. Because the F/A-18C does not experience abrupt stall within its flight envelope, the goal of this research was to determine which of these wing parameters contributed to the abrupt stall phenomenon initially encountered by the F/A-18E.

Computational fluid dynamics (CFD) was used as the tool to accomplish this goal. To determine the effect of each of the wing parameters listed in Table 1, the grid of the F/A-18C was modified or "morphed" to reflect the changes made to these parameters when

Table 1 Comparison of wing parameters on the F/A-18C and F/A-18E

Wing parameter	F/A-18C	F/A-18E
Thickness	3.5 to 5.0% chord	3.8 to 6.2% chord
Camber	0.6% chord	No camber
Twist	4-deg outboard twist	No twist
Snag	No snag	LE snag
Leading-edge (LE) radius	0.08 to 0.31 in.	0.04 in.
LE flap-chord ratio	20% chord	11.3 to 18.1% chord

designing the F/A-18E. For example, to determine the effect of twist on abrupt stall, the twist was removed from the F/A-18C grid to form a morphed grid. The twist was removed from the F/A-18C grid because, as shown in Table 1, the F/A-18C wing has twist while the F/A-18E wing does not. The parameters listed in Table 1 were modified independently and then in combination.

After analyzing each of the configurations at transonic speeds, the wing-root bending-moment (WRBM) coefficient was plotted as a function of angle of attack (AoA). Based on the figures of merit developed during the AWS program,[3] abrupt stall can occur when the slope of the coefficient of WRBM curve changes sign. The AoA at which the slope changes sign is of particular importance. If, for any of the morphed configurations, the slope of the WRBM curve changes sign at a lower AoA than it does for the F/A-18C, then this indicates that the particular wing parameter or parameters being modified might be contributing to abrupt stall.

In the following sections, the CFD grid and flow solver will be discussed. Next, the F/A-18C results from CFD will be compared to the results from the wind-tunnel experiment. Then, the WRBM figure of merit will be discussed as well as the methodology used to accomplish the goal of this research. The CFD analysis of the F/A-18C grid will be presented prior to discussing the results of the morphing study. In the last section, the concluding remarks will be presented.

Numerical Method

The F/A-18C was modeled with a structured, overset grid, which is composed of 79 blocks and approximately 13.9 million points. The baseline F/A-18C grid was constructed under contract by the Boeing Company. The grid size and resolution were determined based on experience gained from similar grid-convergence studies conducted on the F/A-18E previously.[4]

Whereas it is recognized that the wing-drop phenomenon is a result of an abrupt flow separation on one side of the aircraft prior to the other, it was felt that significant flow-physics understanding could be gained by modeling only one side of the aircraft employing a symmetry-plane boundary condition. Modeling the full aircraft would have increased the time and the computer resources required and, therefore, would have rendered this study impractical.

The horizontal and vertical tails are not represented in the grid because it was anticipated that they would have little impact on the abrupt-stall phenomenon encountered by the F/A-18E. The leading- and trailing-edge flaps are deflected to 6 and 8 deg, respectively, whereas the aileron is not deflected. This is referred to as a 6 deg/8 deg/0 deg flap setting. A missile launcher and a Sidewinder missile are attached to the wing tip.

The WIND flow solver[5] was used to obtain the flow solution on the F/A-18C configuration and all of the morphed configurations studied during this project. The turbulence model used during this research was Menter's Shear Stress Transport (SST) model[6] because it was determined early in the AWS program that the solutions on the F/A-18E using Menter's SST correlated well with wind-tunnel results.[2]

The WIND flow solver required 900 MBytes of memory on Silicon Graphics Octanes and Origin 2000/3000/3800 machines, and each solution required approximately 6000 CPU hours to complete. Convergence was achieved when the lift and drag coefficients were unchanged to the fourth significant figure for 100 cycles of the flow solver. While the solution converged, the residual was reduced by at least three orders of magnitude.

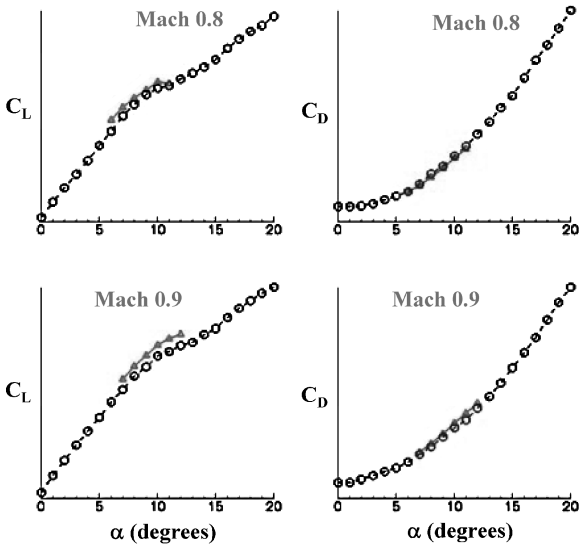

Fig. 1 Comparison of aircraft lift and drag coefficients between CFD and wind-tunnel experiment, with F/A-18C, $Re = 2.07 \times 10^6$, and 6-deg/8-deg/0-deg flaps: ▲, CFD (WIND); and ○, AEDC TC-1029+.

Comparison with Wind-Tunnel Experiment

The F/A-18C grid was analyzed at Mach 0.8 and 0.9 at a Reynolds number of 2.07×10^6 based on the mean aerodynamic chord (MAC) for several AoA, and the results were compared to the wind-tunnel data obtained from the 4-Foot Transonic Propulsion Wind Tunnel at the Arnold Engineering Development Center (AEDC).[7] A Reynolds number of 2.07×10^6 corresponds to the wind-tunnel Reynolds number of 3×10^6/ft for a 6% scale model. In Fig. 1, the lift and drag coefficients from CFD are compared to the wind-tunnel data obtained at the AEDC. In general, the lift and drag coefficients from CFD compare very well with the wind-tunnel data. The lift from CFD does slightly overpredict the wind-tunnel data. This overprediction can probably be explained by the fact that the wind-tunnel model had horizontal and vertical tails, while the CFD grid did not. The wind-tunnel data shown in Fig. 1 were obtained while the horizontal tail deflection angle was 0 deg.

The correlation of the lift and drag between CFD and the wind-tunnel experiment indicate that the grid and flow solver are adequate for accurately predicting the flow over the F/A-18C.

Wing-Root Bending-Moment Coefficient as a Figure of Merit

The WRBM coefficient was utilized as a figure of merit for identifying AWS.[3] The WRBM coefficient is calculated using the equation

$$C_{\mathrm{WB}} = \int_{y_{\mathrm{root}}}^{y_{\mathrm{tip}}} \frac{l(y - y_{\mathrm{ref}})\,\mathrm{d}y}{(q_\infty S_{\mathrm{ref}} b_{\mathrm{ref}})}$$

on the wing of the aircraft. In this equation, y_{ref} was taken to be at the interface between the wing and the leading-edge extension of the F/A-18C.

Based on correlation between wind-tunnel and flight tests, abrupt stall can occur when the slope of the WRBM vs AoA curve changes sign. Abrupt stall, however, is not guaranteed to occur when the slope of the WRBM changes sign. The change in sign could also occur with no significant lateral activity being present. The change in sign suggests that further testing is necessary to determine if there is an unacceptable lateral problem.

Because the change in sign of the slope of the WRBM curve can indicate the onset of the abrupt stall, the AoA where the slope changes sign will be referred to as the onset AoA. The onset AoA specifically refers to the AoA where the sign of the slope changes from positive to negative. The onset AoA indicates the lower boundary of an AWS region of interest, in which abrupt stall could occur. The AWS region of interest extends approximately from the onset

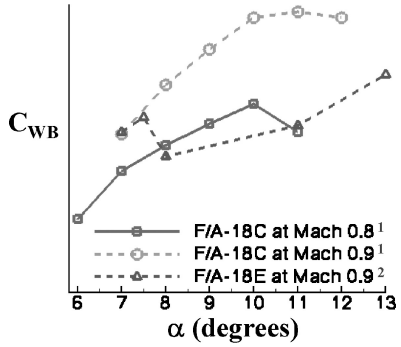

Fig. 2 WRBM coefficient vs AoA from CFD calculations of the F/A-18C and the F/A-18E: 1, $Re = 2.07 \times 10^6$; 6-deg/8-deg/0-deg flaps and 2, $Re = 3.14 \times 10^6$; 6-deg/8-deg/4-deg flaps.

AoA to an AoA where the slope of the WRBM curve becomes positive again. As will be seen later, it is possible for a configuration to have several distinct AWS regions of interest for a given Mach and Reynolds number.

In Fig. 2, the WRBM coefficient is plotted as a function of AoA for the F/A-18C at Mach 0.8 and 0.9 at a Reynolds number of 2.07×10^6 based on MAC and the F/A-18E at Mach 0.9 at a Reynolds number of 3.14×10^6. It can be seen in the figure that the onset AoA for the F/A-18C is 10 deg at Mach 0.8 and 11 deg at Mach 0.9. Although the slope of the WRBM curve changes sign for the F/A-18C with 6-deg/8-deg/0-deg flaps, the flaps are not on schedule at 10 and 11 deg AoA. As a result, the F/A-18C does not experience abrupt stall within its flight envelope.

The preproduction F/A-18E, however, did experience abrupt stall. As can be seen in Fig. 2, the onset AoA for the F/A-18E with 6-deg/8-deg/4-deg flaps is 7.5 deg. Based on this onset AoA, an AWS region of interest is formed between 7.5 and 8 deg. The region of interest extends to 8 deg because the sign of the slope becomes positive again at that AoA. Because the 6 deg/8 deg/4 deg flaps are nearly on schedule in this AWS region of interest, the abrupt stall occurred within the flight envelope of the aircraft.

As just mentioned there is a difference in the Reynolds number between the F/A-18C and the F/A-18E results plotted in Fig. 2. Based on the wind-tunnel tests performed during this program, the AWS characteristics of the F/A-18C and the F/A-18E models are not significantly impacted by Reynolds number.

In Fig. 2 and throughout this paper, the F/A-18C with 6-deg/8-deg/0-deg flaps was compared to the F/A-18E with 6-deg/8-deg/4-deg flaps. The only difference between these two flap settings is that the aileron is not deflected on the F/A-18C, while the aileron is deflected 4 deg downward on the F/A-18E. This difference in flap settings is not contributing significantly to the difference in the AWS characteristics seen between the two aircraft because unpublished Veridian wind-tunnel data indicate that abrupt wing stall is more sensitive to the leading-edge flap setting than it is to the trailing-edge flap and aileron settings. To mimic the flap settings for the F/A-18C grid that was analyzed and compared to wind-tunnel data, the flaps on each of the morphing configurations evaluated during this study were set to 6 deg/8 deg/0 deg.

Methodology

In an effort to determine their impact on abrupt stall, the wing parameters listed in Table 1 were evaluated by modifying the F/A-18C wing to reflect the changes that were made to the wing when designing the F/A-18E. This process of modifying the wing parameters on the F/A-18C wing is referred to as morphing. Eleven different morphing configurations, which are shown in Table 2, were used to determine if the six wing parameters were contributing to the abrupt stall. With six wing parameters being evaluated, it is possible to consider 64 (2^6) different configurations in determining which wing parameters were contributing to the abrupt wing stall. However, analyzing and postprocessing the data for 64 different configurations is impractical given limited budget, time, and computer resources. For this reason, the 11 different morphing configurations considered during this project were chosen carefully, in an attempt to obtain the maximum amount of information from the smallest amount of resources.

Table 2 Morphing configurations used during this research

Morphing configuration	Snag	Thickness	Camber	Twist	LE radius	LE flap-chord ratio
1	X	——	——	——	——	——
2	——	X	——	——	——	——
3	——	——	X	——	——	——
4	——	——	——	X	——	——
5	——	——	——	——	X	——
6	——	——	——	——	——	X
7	X	X	——	——	——	——
8	X	——	X	——	——	——
9	X	——	——	X	——	——
10	X	——	——	——	X	——
11	X	——	——	——	——	X

For the first six morphing cases shown in Table 2, the F/A-18C was modified to reflect the change made for the specific wing parameter. For example, morphing case #4 in Table 2 represents the F/A-18C with an untwisted wing. While removing the twist from the wing, the other wing parameters shown in Table 1 were unchanged. The twist was removed from the F/A-18C wing because the F/A-18E wing is untwisted, as shown in Table 1.

Morphing cases 7–11 in Table 2 represent cases where two wing parameters were modified simultaneously. Specifically, these cases show the effect of the latter five wing parameters on a wing with a snag. For example, morphing case #8 represents a configuration where a snag was added to the F/A-18C wing while at the same time the camber was removed from the wing. The camber was removed from the wing because the F/A-18E wing is uncambered.

After creating the new grids with the desired changes in wing parameters, solutions were generated at Mach 0.8 and 0.9 for several AoAs. The WRBM coefficient was then plotted as a function of AoA to determine which wing parameters were having an effect on abrupt stall.

From Fig. 2, one can see the changes in WRBM coefficient that indicate that a particular wing parameter is contributing to abrupt stall. Because the F/A-18C wing is being morphed to mimic an F/A-18E wing, one should expect that wing parameters contributing to abrupt stall would move the onset AoA in the WRBM curve from the F/A-18C toward the F/A-18E. In particular, the AoA at which the slope changes sign will be reduced from 10 and 11 deg at Mach 0.8 and Mach 0.9 to approximately 7.5-deg AoA or less.

Before presenting the results of the morphing study, the results of the analysis of the F/A-18C will be presented.

Analysis of the F/A-18C

In this section, the baseline F/A-18C results will be discussed. In Figs. 3 and 4, the pressure coefficients, surface-restricted particle traces, and regions of off-body flow reversal on the upper surface of the wing are shown for several AoA at Mach 0.8 and 0.9. The areas above the wing covered in red indicate the regions of flow reversal. As expected, for both Mach numbers the flow separation moves toward the leading edge as the AoA is increased. Because abrupt stall occurs when the amount of flow separation increases rapidly with AoA, analyzing the regions of flow separation and how they change with increasing AoA is important.

In Fig. 5, the sectional lift coefficient and its derivative with AoA are plotted as a function of spanwise location for the F/A-18C at Mach 0.8 and 0.9. It can be seen from the figure that the sectional lift increases over the span until 11 and 12 deg AoA at Mach 0.8 and 0.9, respectively. The discontinuity in the F/A-18C sectional lift plots near $2y/b = 0.67$ is caused by the different deflections between the trailing-edge flap and the aileron. Recall that the WRBM coefficient for the F/A-18C changed sign at 10 and 11 deg for Mach 0.8 and 0.9, respectively. This is consistent with the loss in lift that appears in Fig. 5.

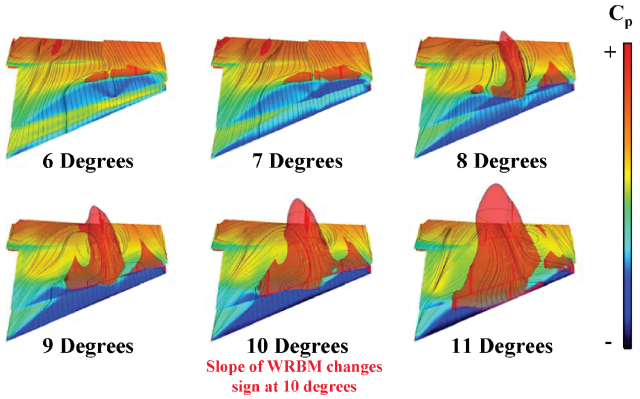

Fig. 3 Pressures, surface-restricted particle traces, and regions of off-body flow reversal for the F/A-18C at Mach 0.8, $Re = 2.07 \times 10^6$, and 6-deg/8-deg/0-deg flaps.

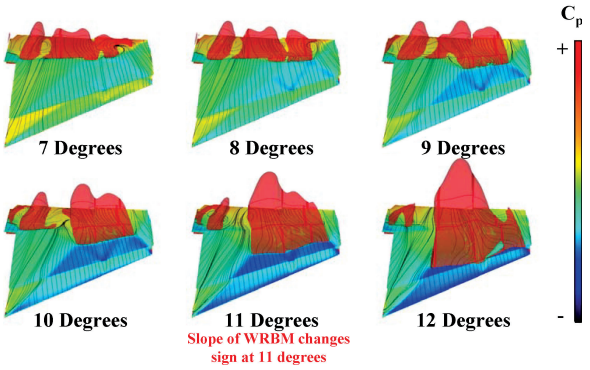

Fig. 4 Pressures, surface-restricted particle traces, and regions of off-body flow reversal for the F/A-18C at Mach 0.9, $Re = 2.07 \times 10^6$, and 6-deg/8-deg/0-deg flaps.

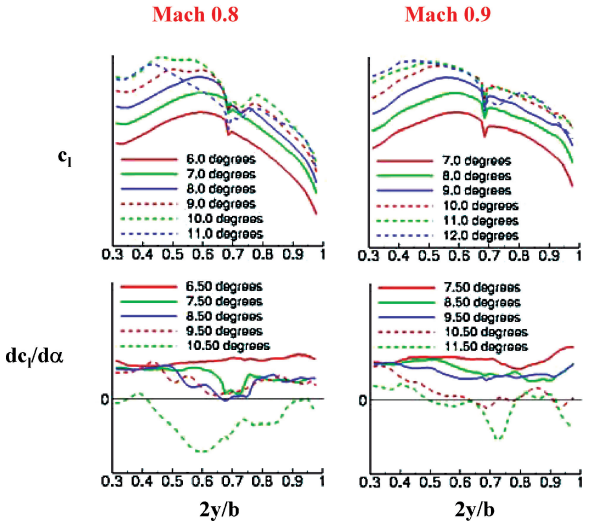

Fig. 5 Sectional lift and its derivative with respect to AoA vs spanwise location for the F/A-18C for various AoA: $Re = 2.07 \times 10^6$ and 6-deg/8-deg/0-deg flaps.

Plots of $dc_l/d\alpha$ yielded valuable information during this research. These plots give insight into the location on the span where lift is being lost. This can help tremendously when determining the factors that are contributing to abrupt stall. Furthermore, there is a good correlation between the AoA where the largest amount of lift is lost on the $dc_l/d\alpha$ plots and the onset AoA from the WRBM curves.

Results

In this section, the results from the morphing study will be presented. In each of the six subsections that follow, the results from a particular wing parameter will be discussed, and conclusions will be drawn about the effect of the wing parameter on abrupt stall.

To help compare the cases, the difference between the onset AoA for each of the morphing configurations and the baseline F/A-18C for Mach 0.8 and 0.9 is shown in Table 3. As an example, the first case listed in the table represents the F/A-18C with reduced leading-edge radius. In general, as one goes from the top to the bottom of the table the difference between the onset AoA of the morphed configuration and the F/A-18C becomes larger.

Table 3 Difference in onset AoA between morphing configurations and the F/A-18C

Morphing configuration	Mach 0.8	Mach 0.9
LE radius	0	0
Twist	−1	0
Camber	−1.5	0
11.3% LE flap-chord ratio	−1	−1
Thickness	−2.5 and 0	−1
Snag	−2	−2
Snag, thickness	−2	−1
Snag, twist	−2	−2
Snag, LE radius	−2	−2
Snag, camber	−2.5	−2.5
Snag with tapered LE flap	−3.5	−3.2

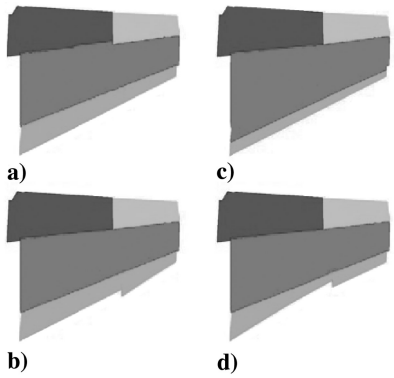

Fig. 6 Wing planforms of a) the F/A-18C, b) F/A-18C with a snag, c) F/A-18C with reduced leading-edge flap-chord ratio, and d) the F/A-18C with a snag and tapered leading-edge flap.

Snag

During the design of the F/A-18E wing, a leading-edge snag was added to the wing to improve the high-lift performance of the aircraft at low speeds. There is no leading-edge snag on the F/A-18C.

During this research, a leading-edge snag was added to the F/A-18C wing to determine its effect on abrupt stall. This case corresponds to morphing case #1 in Table 2. The planform of the F/A-18C wing with a snag is compared to that of the F/A-18C wing in Fig. 6. In this figure, the baseline F/A-18C wing is shown in the upper-left corner, while the F/A-18C wing with a snag is shown in the lower-left corner. The wings are colored to distinguish the leading-edge flap, wing box, trailing-edge flap, and aileron.

The snag was placed at the same nondimensional spanwise location as it is on the F/A-18E. To create the snag, the leading-edge flap of the F/A-18C was extended so that the ratio of the chord length between the airfoil section outboard of the snag and inboard of the snag was identical to that of the F/A-18E. Because the snag was placed near the wing-fold fairing on the F/A-18C, the wing-fold fairing and other protuberances were removed from the wing to simplify the process of adding the snag. With the exception of the wing-fold fairing, the leading-edge flap on the F/A-18C wing was only modified outboard of the snag location. The addition of the snag to the F/A-18C grid resulted in the addition of seven overset blocks and approximately 1.8 million points to the grid.

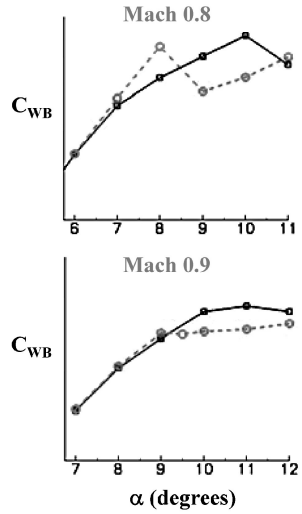

Fig. 7 WRBM coefficient vs AoA for the F/A-18C and F/A-18C with a snag with $Re = 2.07 \times 10^6$ and 6-deg/8-deg/0-deg flaps: □, F/A-18C; and ◇, F/A-18C with snag.

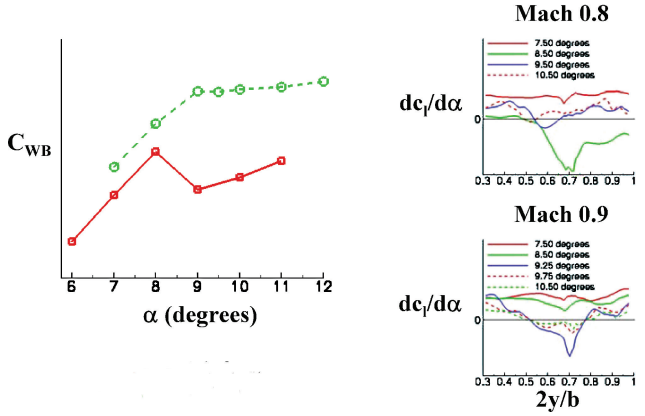

Fig. 8 WRBM coefficient vs AoA and derivative of sectional lift coefficient with respect to AoA vs spanwise location for the F/A-18C with a snag with $Re = 2.07 \times 10^6$ and 6-deg/8-deg/0-deg flaps: □, Mach 0.8; and ◇, Mach 0.9.

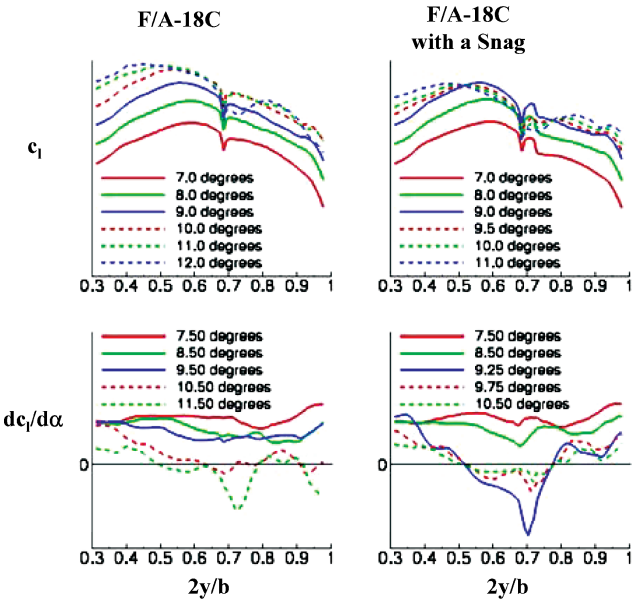

Fig. 9 Sectional lift coefficient and its derivative with respect to AoA as a function of spanwise location for the F/A-18C and F/A-18C with a snag for various AoA: Mach 0.9, $Re = 2.07 \times 10^6$, and 6-deg/8-deg/0-deg flaps.

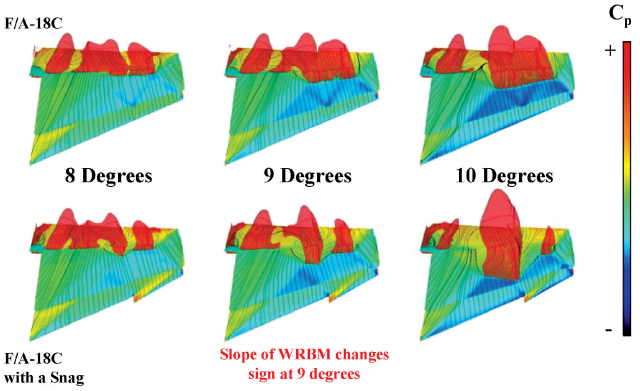

Fig. 10 Pressures, surface-restricted particle traces, and regions of off-body flow reversal for the F/A-18C and F/A-18C with a snag: Mach 0.9, $Re = 2.07 \times 10^6$, and 6-deg/8-deg/0-deg flaps.

The results of WRBM coefficient for the F/A-18C and the F/A-18C with a snag are shown in Fig. 7. It can be seen in the figure that the addition of a snag changes the WRBM curves significantly. At Mach 0.8, the onset AoA for the configuration with a snag is 8 deg. This represents a reduction of 2 deg in the onset AoA from the F/A-18C. At Mach 0.9, the addition of the leading-edge snag reduces the onset AoA by 2 deg from 11 to 9 deg. A 2-deg reduction in the onset AoA is large, and, as a result, the snag is a significant contributor to the abrupt stall initially encountered by the F/A-18E.

The WRBM curves at Mach 0.8 and 0.9 for the F/A-18C with a snag are compared in Fig. 8. These curves differ in character, partially because the WRBM curve at Mach 0.8 has a sharper peak where the slope changes sign. The sharper peak at Mach 0.8 is also manifested by a larger loss in lift in the $dc_l/d\alpha$ curves, which are also shown in Fig. 8. In each of the $dc_l/d\alpha$ plots, the largest loss in lift corresponds to the onset AoA on the WRBM plots. These results indicate that the $dc_l/d\alpha$ curves are useful for predicting the severity of the abrupt stall, in addition to the AoA where the abrupt stall occurs.

The sectional lift and $dc_l/d\alpha$ are plotted as a function of spanwise location for the F/A-18C and F/A-18C with a snag at Mach 0.9 in Fig. 9. The $dc_l/d\alpha$ curves for the F/A-18C with a snag indicate that the largest loss in lift occurs between 9- and 9.5-deg AoA and is centered near the location of the snag. Furthermore, this loss in lift is greater than the F/A-18C experienced between 11- and 12-deg AoA.

In Fig. 10, the pressures, surface-restricted particle traces, and regions of off-body flow reversal on the upper surface of the wing for the F/A-18C and the F/A-18C with a snag are compared at Mach 0.9 for 8-, 9-, and 10-deg AoA. In this figure, the F/A-18C wing is shown on the top while the F/A-18C wing with a snag is shown on the bottom. At 8- and 9-deg AoA, the flow separates at nearly the same location on both wings. However, at 10-deg AoA the flow separation on the wing with a snag has moved further forward than the separation on the F/A-18C. This rapid, forward movement of the flow separation region for the F/A-18C with a snag between 9- and 10-deg AoA is causing the slope to change sign in the WRBM in Fig. 7 and the loss in lift that occurs in Fig. 9.

In Fig. 11, the chordwise pressure distribution is plotted just inboard of the snag for several AoA for the F/A-18C and F/A-18C with a snag at Mach 0.9. For the F/A-18C with a snag, the pressure coefficient is more negative at the leading edge, and the pressure gradient on the leading-edge flap is more adverse than it is on the F/A-18C. Between 9- and 12-deg AoA, the shock on the upper surface of the F/A-18C with a snag moves forward more rapidly than it does on the F/A-18C. At 12-deg AoA, the flow separation has reached the leading edge of the wing with a snag.

As just mentioned, the leading-edge snag is contributing significantly to abrupt stall at both flow conditions considered. The reason that the snag is contributing to abrupt stall is shown in Figs. 12 and 13. The particle traces near the snag on the F/A-18C with a snag configuration are shown in Fig. 12. As the flow accelerates around the inboard edge of the snag, a region of low pressure is formed

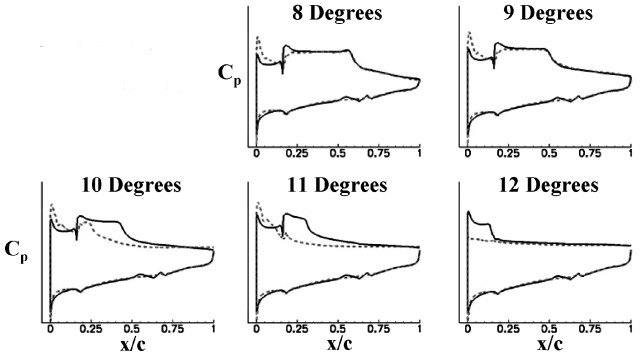

Fig. 11 Effect of the snag on the chordwise pressure distribution just inboard of the snag with Mach 0.9, $Re = 2.07 \times 10^6$, and 6-deg/8-deg/0-deg flaps inboard of snag at $2y/b = 0.7222$: ——, F/A-18C; and - - - -, F/A-18C with snag.

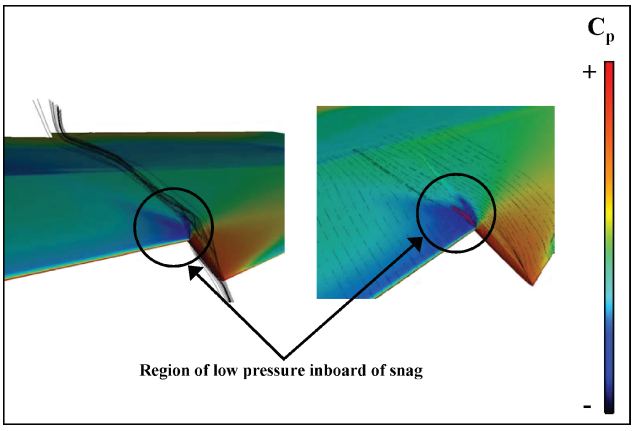

Fig. 12 Particle traces near the snag on the F/A-18C with a snag.

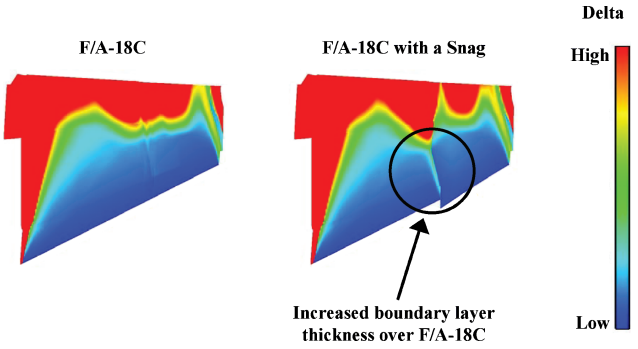

Fig. 13 Typical contours of boundary-layer thickness on the upper surface of the F/A-18C and F/A-18C with a snag.

on the upper surface of the leading-edge flap inboard of the snag. This region of low pressure causes a steep adverse pressure gradient, which separates the flow on the flap inboard of the snag. The region of reversed flow is shown in red on the right-hand plot in Fig. 12. As a result of the adverse pressure gradient and flap separation, the boundary layer thickens and separates earlier on the wing. A typical plot of the contours of boundary-layer thickness for the F/A-18C and F/A-18C with a snag is shown in Fig. 13. In this figure, the boundary layer becomes thicker as the color changes from blue to red. For the F/A-18C with a snag, the boundary layer starts thickening on the leading-edge flap just inboard of the snag.

Because the addition of a leading-edge snag to the F/A-18C wing reduced the onset AoA by 2 deg at both Mach 0.8 and 0.9, the camber, thickness, twist, leading-edge radius, and leading-edge flap-chord ratio on the F/A-18C were modified independently and then in combination with the leading-edge snag. The results for these five wing parameters in combination with the snag are compared to the results of the F/A-18C with the snag discussed in this section.

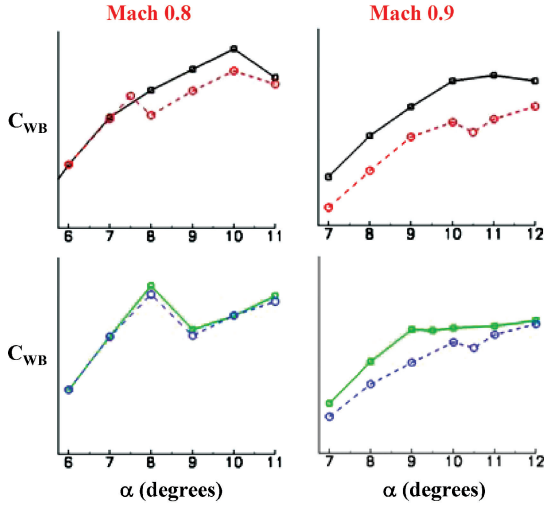

Fig. 14 Effect on the WRBM coefficient of increasing the thickness on the F/A-18C wing and F/A-18C wing with a snag with $Re = 2.07 \times 10^6$ and 6-deg/8-deg/0-deg flaps: ——, F/A-18C; - - -○- - -, F/A-18C with thickened wing; ——, F/A-18C with snag; and - - -○- - -, F/A-18C with snag and thickened wing.

Thickness

The effect of thickness on abrupt stall was determined by analyzing two different configurations, as shown in Table 2. In the first case, the thickness of the F/A-18C wing was increased, as indicated in Table 1. In the upper two plots of Fig. 14, the WRBM coefficient is shown as a function of AoA for the F/A-18C and the F/A-18C with a thickened wing for Mach 0.8 and 0.9. At Mach 0.8, the slope changes sign at 7.5 and 10 deg for the thickened wing. As a result, two distinct AWS regions of interest are present. While one region extends from 7.5 to 8 deg, the other region extends from 10- to 11-deg AoA. The change in sign at 7.5 deg represents a 2.5-deg reduction in onset AoA from the F/A-18C. At Mach 0.9, the slope changed sign at 10 deg for the thickened wing. This represents a 1-deg reduction from the F/A-18C.

For the second case, the F/A-18C was modified by adding a leading-edge snag and thickening the wing. The WRBM for this configuration is compared to that of the F/A-18C with a snag at Mach 0.8 and 0.9 in the lower two plots Fig. 14. At Mach 0.8, the increase in thickness does not change the onset AoA. At Mach 0.9, however, the onset AoA increases by 1 deg as a result of the increase in wing thickness. This was the only case examined during this study where a change in a wing parameter increased the onset AoA.

Based on these results, thickness does not appear to be contributing to abrupt stall on the F/A-18E.

Camber

Morphing cases 3 and 8 in Table 2 were used to analyze the effect of camber on abrupt stall. In the first case, the camber was removed from the F/A-18C wing. In the second case, the camber was removed from the F/A-18C wing while also adding a leading-edge snag. The WRBM curves for these cases at Mach 0.8 and 0.9 are shown in Fig. 15. The results for the first case are shown in the plots at the top, where the WRBM curves for the F/A-18C with an uncambered wing are compared to that of the F/A-18C. These results indicate that the removal of the camber from the F/A-18C wing reduced the onset AoA by 1.5 deg at Mach 0.8. The removal of the camber from the wing does not change the onset AoA at Mach 0.9.

The results for the second case are shown in the plots at the bottom of Fig. 15. In these plots, the WRBM curves for the F/A-18C with a snag and uncambered wing are compared to those of the F/A-18C with a snag for Mach 0.8 and 0.9. These two plots indicate that removal of the camber from the wing with a snag reduces the onset AoA by 0.5 deg at both Mach numbers.

Based on these results, the removal of the camber from the wing could be a contributing factor to AWS. A possible explanation for

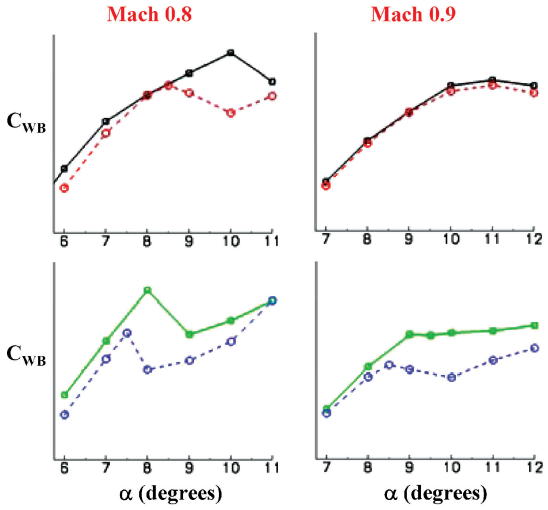

Fig. 15 Effect on the WRBM coefficient of removing the camber from the F/A-18C wing and the F/A-18C wing with a snag with $Re = 2.07 \times 10^6$ and 6-deg/8-deg/0-deg flaps: ——●——, F/A-18C; - - -○- - -, F/A-18C with uncambered wing; ——●——, F/A-18C with snag; and - - -○- - -, F/A-18 with snag and uncambered wing.

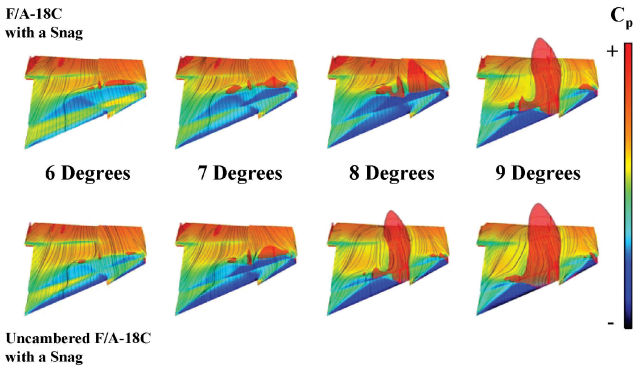

Fig. 16 Pressures, surface-restricted particle traces, and regions of off-body flow reversal for the F/A-18C with a snag and F/A-18C with a snag and uncambered wing: Mach 0.8, $Re = 2.07 \times 10^6$, and 6-deg/8-deg/0-deg flaps.

the contribution of the camber to abrupt stall can be seen in Fig. 16. In this figure, the upper surface-pressure contours, surface-restricted particle traces, and regions of flow reversal for the F/A-18C with a snag and the F/A-18C with a snag and uncambered wing are shown at Mach 0.8 for several AoA. In this figure, the 6-, 7-, and 8-deg uncambered cases appear to be very similar to the 7-, 8-, and 9-deg cambered cases. This shift in AoA is probably being caused by the increased loading on the leading-edge flap that results from uncambering the flap. The removal of the camber from the flap increases the relative AoA between the mean-camber line of the flap and the oncoming flow.

Twist

The effect of twist on abrupt stall was determined by analyzing two different configurations. These cases are shown as morphing cases 4 and 9 in Table 2. In the first case, the twist was removed from the F/A-18C wing. In the second case, a leading-edge snag was added to the F/A-18C wing while removing the twist from the wing. The WRBM is shown as a function of AoA for both cases in Fig. 17. The two upper plots show the results of the first case, while the two lower plots show the results of the second case. Although removing the twist from the F/A-18C wing reduced the onset AoA by 1 deg at Mach 0.8, the removal of the twist did not shift the onset AoA at Mach 0.9. Furthermore, after adding a snag to the wing, removing the twist did not change the onset AoA at Mach 0.8 or 0.9. These results indicate that the removal of the twist is not contributing to abrupt stall on the F/A-18E.

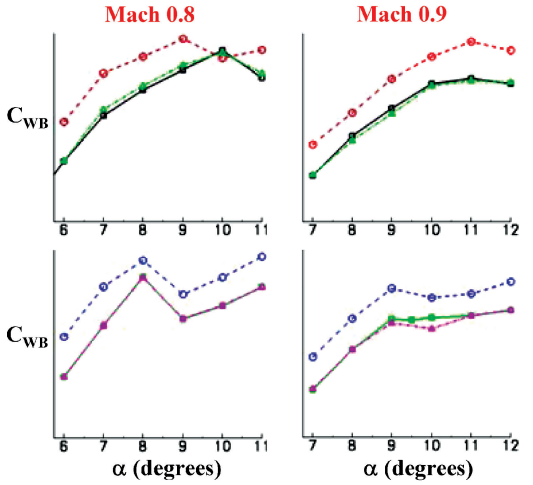

Fig. 17 Effect on the WRBM coefficient of removing the twist and reducing the leading-edge radius on the F/A-18C wing and the F/A-18C wing with a snag with $Re = 2.07 \times 10^6$ and 6-deg/8-deg/0-deg flaps: ——●——, F/A-18C; - - -○- - -, F/A-18C with untwisted wing; -·-·-, F/A-18C with reduced LE radius; ——●——, F/A-18C with snag; - - -○- - -, F/A-18 with snag and untwisted wing; and -·-·-, F/A-18C with snag and reduced LE radius.

Leading-Edge Radius

The effect of leading-edge radius on abrupt stall was also investigated in this study. As shown in Table 1, the leading-edge radius on the F/A-18E is smaller than that on the F/A-18C. Two different configurations were analyzed to determine the effect of leading-edge radius. These cases correspond to morphing cases 5 and 10 in Table 2. In the first case, the leading-edge radius of the F/A-18C was reduced to match that of the F/A-18E. In the second case, a leading-edge snag was added to the F/A-18C while reducing the leading-edge radius of the wing. The WRBM coefficient for both cases is shown in Fig. 17. In this figure, the results from the first case are shown on the top while the results of the second case are shown on the bottom. The plots of WRBM in this figure indicate that reducing the leading-edge radius does not shift the onset AoA. As a result, the reduction of the leading-edge radius does not appear to be a contributing factor to AWS.

Leading-Edge Flap-Chord Ratio

The effect of the leading-edge flap-chord ratio on abrupt stall was also investigated using two different configurations. In the first case, the hinge line on the F/A-18C was moved from 20% chord to 11.3% chord. This was accomplished without changing the planform shape of the F/A-18C. The planform of the F/A-18C wing with reduced leading-edge flap-chord ratio is compared to the F/A-18C wing in Fig. 6. The F/A-18C wing with reduced leading-edge flap-chord ratio is shown in the upper-right corner of the figure. A flap-chord ratio of 11.3% was chosen because the flap-chord ratio on the F/A-18E immediately inboard of the snag is 11.3%. This represents the smallest leading-edge flap-chord ratio on the F/A-18E.

In the upper two plots of Fig. 18, the WRBM for this case is compared to that of the F/A-18C for Mach 0.8 and 0.9. At both Mach numbers, the onset AoA is reduced by 1 deg as a result of the reduction in leading-edge flap-chord ratio. The change in slope is very distinguishable at Mach 0.9, whereas at Mach 0.8 the slope change is less apparent.

The pressure contours, surface-restricted particle traces and regions of flow reversal of the F/A-18C with reduced leading-edge flap-chord ratio are compared to those of the F/A-18C at Mach 0.8 in Fig. 19. The flow separation on the wing with reduced leading-edge flap-chord ratio moves rapidly to the leading edge between 9- and 10-deg AoA. The flow separation on the F/A-18C between 8- and 10-deg AoA is gradually moving forward and still has not reached the leading edge at 10 deg.

In the second configuration, the leading-edge flap of the F/A-18C was modified to include a snag and change the leading-edge

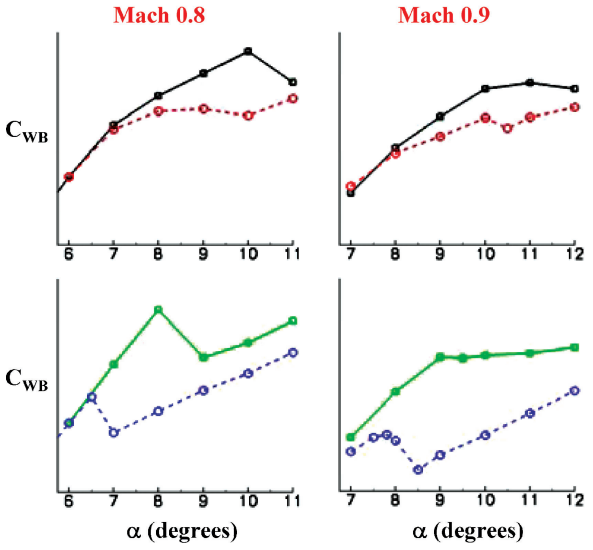

Fig. 18 WRBM coefficient vs AoA for the F/A-18C and F/A-18C with 11.3% leading-edge flap-chord ratio with $Re = 2.07 \times 10^6$ and 6-deg/8-deg/0-deg flaps: ——, F/A-18C; - - -, F/A-18C with 11.3% LE flap-chord ratio; ——, F/A-18C with snag; and - - -, F/A-18 with snag and tapered LE flap.

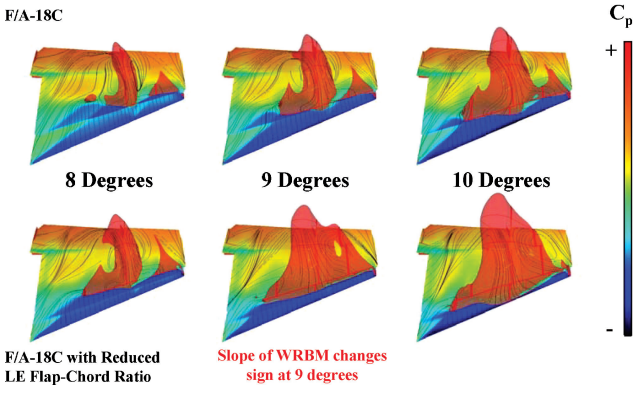

Fig. 19 Pressures, surface-restricted particle traces, and regions of off-body flow reversal for the F/A-18C and F/A-18C with reduced leading-edge flap-chord ratio: Mach 0.8, $Re = 2.07 \times 10^6$, and 6-deg/8-deg/0-deg flaps.

flap-chord ratio simultaneously. This results in a wing with a tapered leading-edge flap. The planform of the F/A-18C wing with a snag and tapered leading-edge flap is shown in the lower-right corner of Fig. 6. The snag was once again placed at the same nondimensional spanwise location as it is on the F/A-18E. The leading-edge flap was modified so that the flap-chord ratio immediately inboard of the snag is 11.3%, just as it is on the F/A-18E. Also, the ratio of the chord length between the airfoil section outboard of the snag and inboard of the snag reflects that on the F/A-18E. At the root and tip of the wing, the leading-edge flap-chord ratio is 20%, which is unchanged from the F/A-18C.

To show the effect of leading-edge flap-chord ratio on a wing with a snag, the WRBM coefficients for the F/A-18C wing with a snag and tapered leading-edge flap are compared to those of the F/A-18C with a snag at Mach 0.8 and 0.9 in the lower two plots in Fig. 18. In this figure, one can see that the onset AoA is reduced by 1.5 deg at Mach 0.8 and 1.2 deg at Mach 0.9 when the leading-edge flap-chord ratio is reduced to 11.3% on the F/A-18C wing with a snag. This implies that when a snag is added to the F/A-18C and the leading-edge flap-chord ratio is reduced simultaneously the onset AoA is reduced from the F/A-18C by 3.5 deg at Mach 0.8 and 3.2 deg at Mach 0.9. Recall from Fig. 1 that the onset AoA for the F/A-18C is 10- and 11-deg AoA at Mach 0.8 and 0.9, respectively. Based on

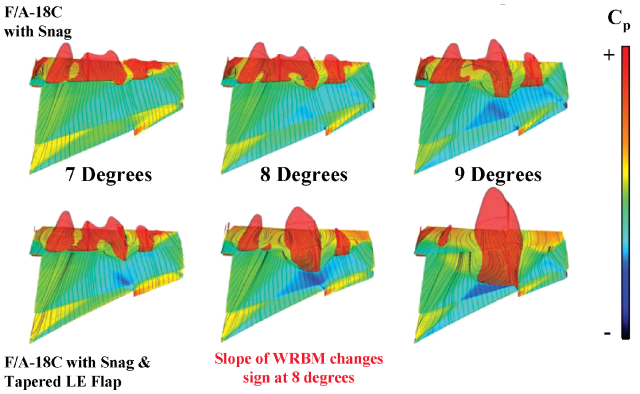

Fig. 20 Pressures, surface-restricted particle traces, and regions of flow reversal for the F/A-18C with a snag and F/A-18C with a snag and tapered leading-edge flap: Mach 09, $Re = 2.07 \times 10^6$, and 6-deg/8-deg/0-deg flaps.

these results, the reduction of the leading-edge flap-chord ratio is contributing significantly to AWS.

The pressure contours, surface-restricted particle traces, and regions of flow reversal of the F/A-18C with a snag and tapered leading-edge flap are compared to those of the F/A-18C with a snag at Mach 0.9 in Fig. 20. The flow separation on the wing with a snag and tapered leading-edge flap moves forward at a more rapid rate between 7 and 9 deg than it does on the F/A-18C wing with a snag. This rapid movement of the flow separation region causes the slope of the WRBM curve to change sign at 7.8 deg, as shown in Fig. 18.

The sectional lift and $dc_l/d\alpha$ for the F/A-18C, F/A-18C with a snag, F/A-18C with a snag and tapered leading-edge flap, and the F/A-18E at Mach 0.9 are shown in Fig. 21. The largest loss in lift on the F/A-18C with a snag and tapered leading-edge flap occurs between 7.8- and 8.5-deg AoA, while the largest loss in lift on the F/A-18E occurs between 7.5- and 8-deg AoA.

As was already mentioned, the reduction of the leading-edge flap-chord ratio is contributing significantly to AWS. The chordwise pressure distribution shown in Fig. 22 gives insight into how the flap-chord ratio is contributing to abrupt stall. In this figure, a comparison is made between the chordwise pressures on the F/A-18C and the F/A-18C with 11.3% leading-edge flap-chord ratio. Recall from Table 1 that the F/A-18C has a leading-edge flap-chord ratio of 20%. In Fig. 22, on the upper surface the flow decelerates on the leading-edge flap from the leading edge to the hinge line. When the length of the leading-edge flap is reduced, the flow has less length to decelerate and, as a result, is moving faster when it encounters the hinge line. The faster velocity upstream of the hinge line accelerates around the hinge line. As a result of the reduced leading-edge flap length and increased velocity after the hinge line, shock-induced flow separation occurs earlier on the wing.

Summary of Results

The difference between the onset AoA of each morphing configuration and the baseline F/A-18C is shown in Table 3 for Mach 0.8 and 0.9. The results in this figure were used to determine that the camber could be contributing to the abrupt stall encountered by the preproduction F/A-18E, while the snag and reduced leading-edge flap-chord ratio are contributing significantly to the abrupt stall.

Since the addition of the leading-edge snag to the F/A-18C wing reduced the onset AoA of AWS by 2 deg, the addition of the snag was determined to be a significant contributor to the abrupt stall. The question used to determine whether the other five wing parameters were contributing to abrupt stall was: "When the wing parameter is modified in combination with a leading-edge snag, is the onset AoA reduced beyond that of the F/A-18C with a snag?" If the answer to this question was yes, then the wing parameter was considered to be contributing to the abrupt stall. The only two wing parameters that fall into this category were the camber and leading-edge flap-chord ratio.

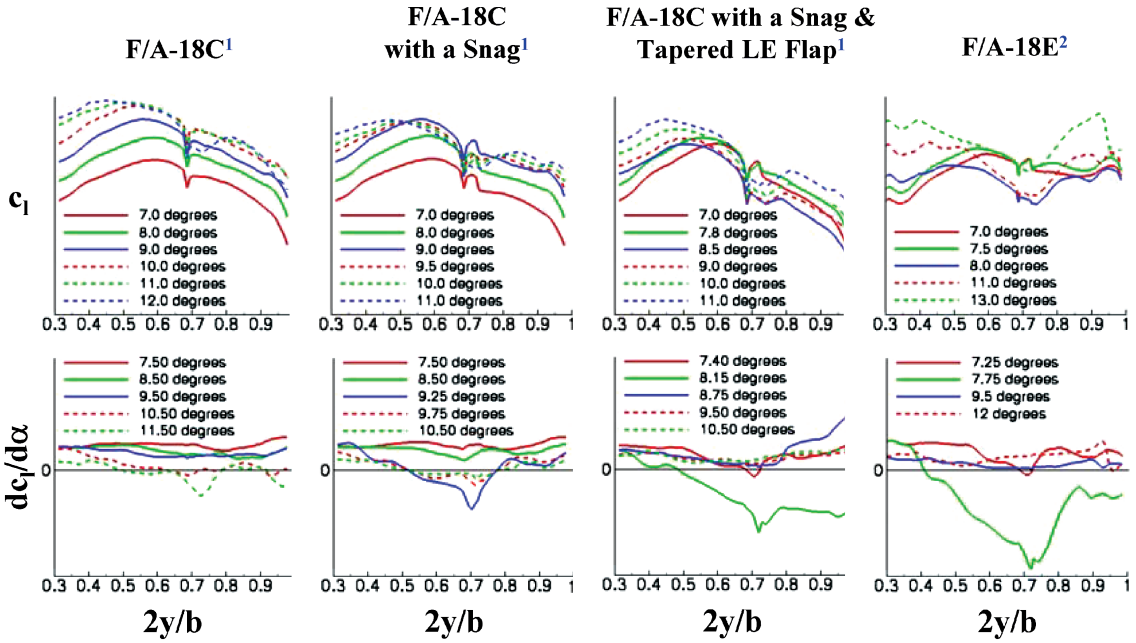

Fig. 21 Sectional lift and its derivative with respect to AoA vs spanwise location for the F/A-18C, F/A-18C with a snag, F/A-18C with a snag and tapered leading-edge flap, and F/A-18E for various AoA: 1, Mach 0.9, $Re = 2.07 \times 10^6$, 6-deg/8-deg/0-deg flaps; and 2, Mach 0.9, $Re = 3.14 \times 10^6$, 6-deg/8-deg/4-deg flaps.

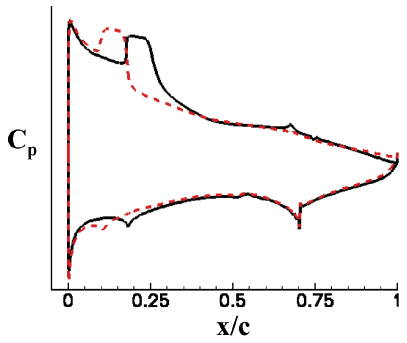

Fig. 22 Typical chordwise pressure distribution for the F/A-18C and F/A-18C with 11.3% leading-edge flap-chord ratio: ——, F/A-18C; and - - - -, F/A-18C with 11.3% LE flap-chord ratio.

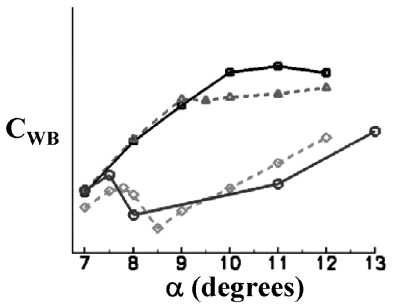

Fig. 23 WRBM coefficient vs AoA for the F/A-18C, F/A-18C with a snag, F/A-18C with a snag and tapered leading-edge flap, and F/A-18E: ——, F/A-18C[1]; - - -◇- - -, F/A-18C with snag[1]; - - -◇- - -, F/A-18C with snag and tapered LE flap[1]; and ——, F/A-18E[2], where 1, Mach 0.9, $Re = 2.07 \times 10^6$, 6-deg/8-deg/0-deg flaps; and 2, Mach 0.9, $Re = 3.14 \times 10^6$, 6-deg/8-deg/4-deg flaps.

When adding a leading-edge snag to the F/A-18C wing and reducing the leading-edge flap-chord ratio, the onset AoA is reduced by 3.5 deg at Mach 0.8 and 3.2 deg at Mach 0.9. The WRBM is plotted as a function of AoA for the F/A-18C, F/A-18C with a snag, F/A-18C with a snag and tapered leading-edge flap, and the F/A-18E at Mach 0.9 in Fig. 23. This figure clearly shows that by adding a snag to the F/A-18C and reducing the leading-edge flap-chord ratio the WRBM curve resembles that of the F/A-18E. The onset AoA is 7.8 deg for the F/A-18C with a snag and tapered leading-edge flap and 7.5 deg for the F/A-18E. This figure reemphasizes that the snag and leading-edge flap-chord ratio are determined to be the major geometric contributors to the abrupt stall on the F/A-18E.

Although it would be possible to consider the impact of changing the camber, twist, thickness, and leading-edge radius on the F/A-18C wing with a snag and tapered leading-edge flap, the time schedule for this project prohibited these calculations. Although it is probable that a change in the camber, twist, thickness, and leading-edge radius would cause a change in the WRBM curve for the F/A-18C with a snag and tapered leading-edge flap in Fig. 23, it is anticipated that the onset AoA of the curve would not change significantly because there is only a 0.3-deg difference between the onset AoA of the F/A-18C with a snag and tapered leading-edge flap and the F/A-18E.

Conclusions

Several wing parameters of the F/A-18C wing have been modified to reflect the changes incorporated in the design of the preproduction F/A-18E. This computational effort was undertaken as part of the abrupt-wing-stall (AWS) program to determine the wing parameters that contributed to the abrupt-stall characteristics initially encountered by the pre-production F/A-18E during flight tests. The knowledge gained from this research could be used by designers of future aircraft to avoid AWS.

The effects of thickness, camber, twist, leading-edge radius, leading-edge flap-chord ratio, and a leading-edge snag on abrupt stall were studied during this project using 11 different morphed configurations. The wing-root bending-moment (WRBM) coefficient was plotted as a function of AoA to determine which wing parameters contributed to AWS on the preproduction F/A-18E.

The results of this research indicate that the addition of a leading-edge snag and the reduction of the leading-edge flap-chord ratio are the primary contributors to AWS. In addition, the removal of the camber from the wing might also be contributing to the abrupt stall. The thickness, twist, and leading-edge radius, however, do not appear to be contributing to the abrupt stall.

The derivative of the sectional lift coefficient with respect to AoA was also investigated as a potential figure of merit (FOM). There

is good correlation between the AoA where the largest loss in lift occurs on the wing and the onset AoA from the WRBM curves. The derivative of sectional lift also indicates the spanwise location where lift is being lost. Furthermore, the derivative of sectional lift with AoA also illustrates a larger lift loss on the wing when the slope of the WRBM curve changes more abruptly. Additional research is needed to determine whether the derivative of sectional lift with respect to AoA can be used as a reliable FOM for lateral activity for future programs.

Acknowledgments

The authors wish to acknowledge Shawn Woodson, Robert Hall, Joseph Chambers, Joseph Laiosa, and Darren Grove for their guidance during this project. In addition, the authors wish to acknowledge the Office of Naval Research for funding this project. Also, the authors wish to acknowledge the Department of Defense High Performance Computing Modernization Program for providing the computer resources necessary to perform this task. Specifically, the computers at the U.S. Army Engineering Research and Development Center, Army Research Laboratory, Aeronautical Systems Center, Naval Research Laboratory, and Space and Missile Defense Command were invaluable.

References

[1]Hall, R. M., and Woodson, S. H., "Introduction to the Abrupt Wing Stall Program," *Journal of Aircraft*, Vol. 41, No. 3, 2004, pp. 425–435.

[2]Grove, D. V., Laiosa, J. P., Woodson, S. H., and Stookesberry, D. C., "Computational Fluid Dynamics Study of an Abrupt Wing Stall Phenomena on the F/A-18E," AIAA Paper 2002-1025, Jan. 2002.

[3]Lamar, J. E., and Hall, R. M., "AWS Figure of Merit (FOM) Developed Parameters from Static Tests," AIAA Paper 2003-0745, Jan. 2003.

[4]Stookesberry, D. C., "CFD Modeling of F/A-18E/F Abrupt Wing Stall—A Discussion of Lessons Learned," AIAA Paper 2001-2662, June 2001.

[5]Bush, R. H., Tower, G. D., and Towne, C. E., "WIND: The Production Flow Solver of the NPARC Alliance," AIAA Paper 1998-0935, Jan. 1998.

[6]Menter, F. R., "Zonal Two Equation k–ω Turbulence Models for Aerodynamic Flows," AIAA Paper 1993-2906, July 1993.

[7]Lyerla, G. W., "F/A-18C Flow Visualization Wind Tunnel Test in AEDC 4-Ft Transonic PWT, Test No. TC-1029+," BOEING-STL 99A0026, The Boeing Company, St. Louis, MO, Aug. 1999.